



**Fermi National Accelerator Laboratory**

**FERMILAB-Conf-90/17-E**  
**[E-741/CDF]**

## **$J/\psi$ and $\gamma$ Production at CDF\***

The CDF Collaboration

*presented by*

Tony Liss  
*University of Illinois*  
*Urbana, Illinois 61801*

January 1990

\* Published in the proceedings of the 8th Topical Workshop on  $p\bar{p}$  Collider Physics, Castiglione della Pescaia, Italy, September 1-5, 1989.



# J/ $\psi$ and $\Upsilon$ Production at CDF

## The CDF Collaboration<sup>†</sup>

Presented by  
 Tony Liss  
 University of Illinois

### Abstract

Characteristics of J/ $\psi$  and  $\Upsilon$  produced at the Tevatron and detected in the dimuon channel at CDF are reviewed. The masses of the J/ $\psi$  and  $\Upsilon$  are measured to be  $3.096 \pm 0.001$  GeV/c<sup>2</sup> and  $9.469 \pm 0.010$  GeV/c<sup>2</sup> respectively. These mass measurements are used to determine the systematic uncertainty on the momentum scale in the central tracking chamber.

## 1 INTRODUCTION

In this paper we report on the characteristics of J/ $\psi$  and  $\Upsilon$  events detected in the CDF central muon system. The CDF detector has been described elsewhere [1]. Here we describe, briefly, only those components used in this analysis. A vertex time-projection chamber (VTPC) close to the beam pipe is used to measure the event z-vertex position. The central tracking chamber (CTC) surrounds the VTPC and allows reconstruction of tracks in three dimensions. A superconducting solenoid encloses these tracking chambers. Outside of the solenoid in the central region is a projective tower calorimeter consisting of separate electromagnetic and hadronic compartments with a tower size of  $\Delta\phi=15^\circ$  and  $\Delta\eta=0.1$ , where  $\eta$  is the pseudo-rapidity. Behind the approximately 5 interaction lengths of calorimeter and covering the pseudo-rapidity range  $|\eta| < 0.65$  is the central muon detector. The central muon detector consists of 4 layers of drift chambers with alternate pairs of wires projecting back to the interaction vertex.

## 2 TRIGGERING ON DIMUONS

The data used in this analysis were taken with a two-level dimuon trigger. Because of the projective nature of the wires in the muon chambers, the slope,  $\alpha$ , of the track segment in the chambers (stub) is inversely proportional to  $P_t$ , according to  $\alpha = 0.14P_t^{-1}$  ( $P_t$  in GeV/c). For nearly all of the data used here, the level 1 trigger was made by requiring a stub with  $P_t > 5$  GeV/c. Approximately 2/3 of the data from the entire run was taken with a level 1  $P_t$  threshold of 3 GeV/c, but only a very small amount of that data appears in this analysis.

At level 2, the dimuon trigger involves matching a muon stub with a track found by a hardware track processor. The trigger for nearly all of the data used here required a track processor  $P_t > 5$  GeV/c pointing at a muon chamber with a stub in it, in addition to at least one other muon stub with a  $P_t > 2$  GeV/c as measured by the stub slope

---

<sup>†</sup>ANL-Brandeis-University of Chicago- Fermilab-INFN, Frascati-Harvard-University of Illinois-KEK-LBL-University of Pennsylvania-INFN, University and Scuola Normale Superiore of Pisa- Purdue-Rockefeller-Rutgers-Texas A& M-Tsukuba-Tufts-University of Wisconsin

Pub. Proceedings 8th Topical Workshop on Proton-Antiproton Collider Physics, Castiglione, Italy, September 1-5, 1989.

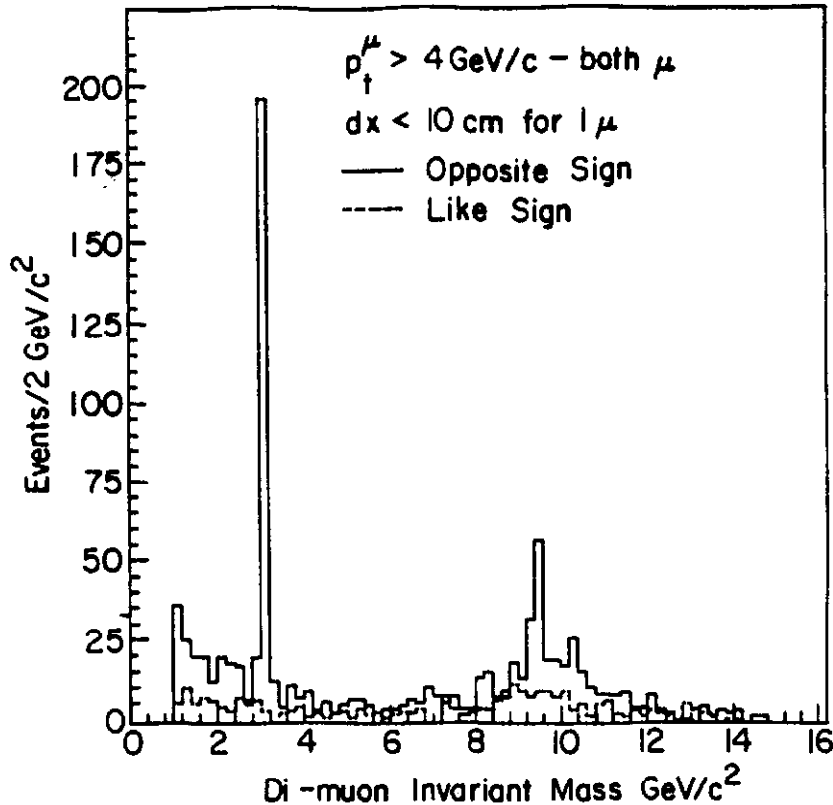


Figure 1: Dimuon Invariant Mass spectrum

only. Approximately 2/3 of the entire run's data was taken with a level 2 trigger which required two muon stubs both of which were matched to tracks with a processor  $P_t > 3$  GeV/c, but very little of that data is used in this analysis.

### 3 DIMUON DATA

Figure 1 shows an invariant mass spectrum from  $1.7\text{pb}^{-1}$  of dimuon data. Each muon was required to have  $P_t > 4$  GeV/c and at least one of the muons was required to have  $DX < 10\text{cm}$ , where DX is the match in the drift direction between the muon stub and an extrapolated CTC track. A very prominent  $J/\psi$  peak is clearly visible and a large enhancement in the  $\Upsilon$  region is also apparent.

#### 3.1 $J/\psi$ Sample Characteristics

Because the  $J/\psi$  events stick out so clearly in Fig. 1, we have elected to study these events without the bias of an offline  $P_t$  cut. Therefore, the  $P_t$  cut was removed and the  $J/\psi$  sample was obtained simply by requiring  $DX < 10\text{cm}$  for each muon. The DX distribution for muons with an invariant mass between 2.8 and 3.4 GeV/c<sup>2</sup> is shown in Figure 2. The  $J/\psi$  sample is defined to be dimuons with masses between 3.0 and 3.2 GeV/c<sup>2</sup>, where both muons satisfy the DX cut. Figures 3 and 4 show, respectively, the distribution of the highest  $P_t$  of the two muons and the distribution of the  $P_t$  of the  $J/\psi$  itself. Figure 3 shows clearly the turn on of the muon trigger at about 5 GeV/c. The small amount of lower threshold data included here can be seen below the 5 GeV/c

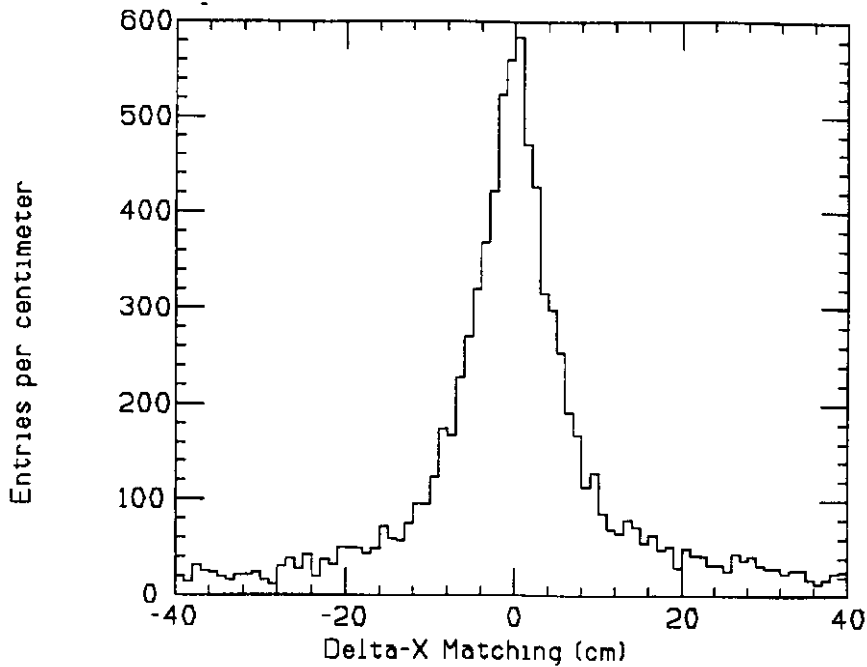


Figure 2: DX distribution for muons from  $J/\psi$  decays

threshold. The mean  $P_t$  of the leading muon is 6.5 GeV/c while the mean  $P_t$  of the  $J/\psi$  itself is approximately 9.0 GeV/c. This indicates that we are observing primarily production of highly boosted  $J/\psi$ s, which is easily understood as a result of the trigger bias. The richness of the  $J/\psi$  sample is an indication that the total production cross section must be extremely high.

### 3.2 $\Upsilon$ Sample Characteristics

In order to enhance the significance of the  $\Upsilon$  events seen in Fig. 1 and to separate mass peaks of  $\Upsilon$  and  $\Upsilon'$  we have made tighter cuts to enhance the quality of the dimuons in the  $\Upsilon$  mass region. In addition to the  $DX < 10$  cm cut used above, we required the following of both muons:  $P_t > 4$  GeV/c, energies deposited in the hadronic and electromagnetic calorimeters less than 3 GeV and 1 GeV, respectively, and the total energy deposited in the eight calorimeter towers surrounding the tower traversed by the muon less than 3 GeV. From test beam data, a muon deposits, on average, slightly less than 2 GeV in the calorimeter (electromagnetic plus hadronic), and 95% of muons deposit less than 6 GeV.

In Figure 5 we show the distribution of the highest  $P_t$  of the two muons for  $\Upsilon$  candidates (invariant masses between 9.0 and 9.8 GeV/c<sup>2</sup>), and in Figure 6 we show the reconstructed  $P_t$  of the  $\Upsilon$  itself. From these two figures we can see that the trigger bias is not nearly so severe for dimuons in the  $\Upsilon$  region, and in fact we do observe  $\Upsilon$ s produced nearly at rest.

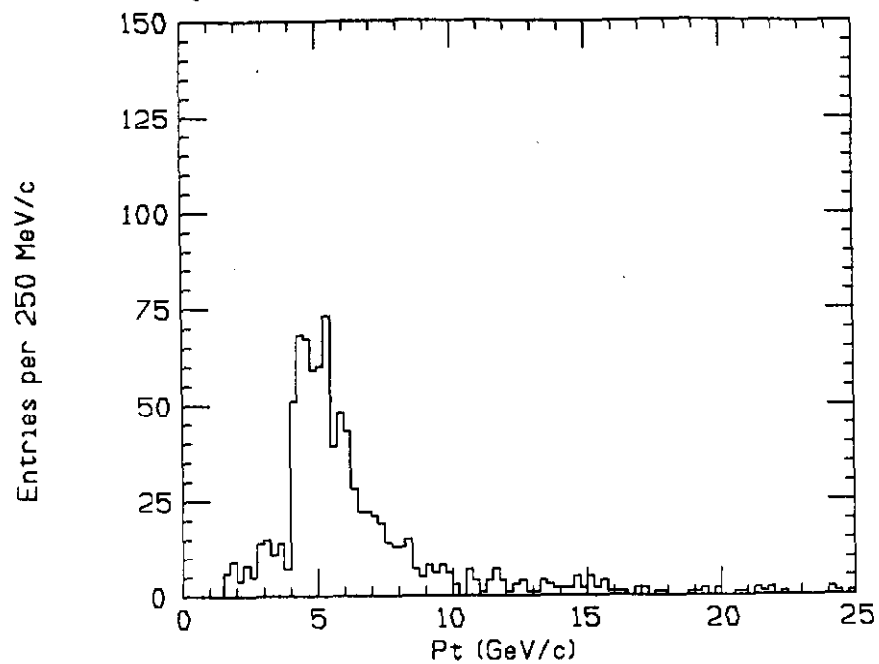


Figure 3: Highest muon  $P_t$  from  $J/\psi$  decays

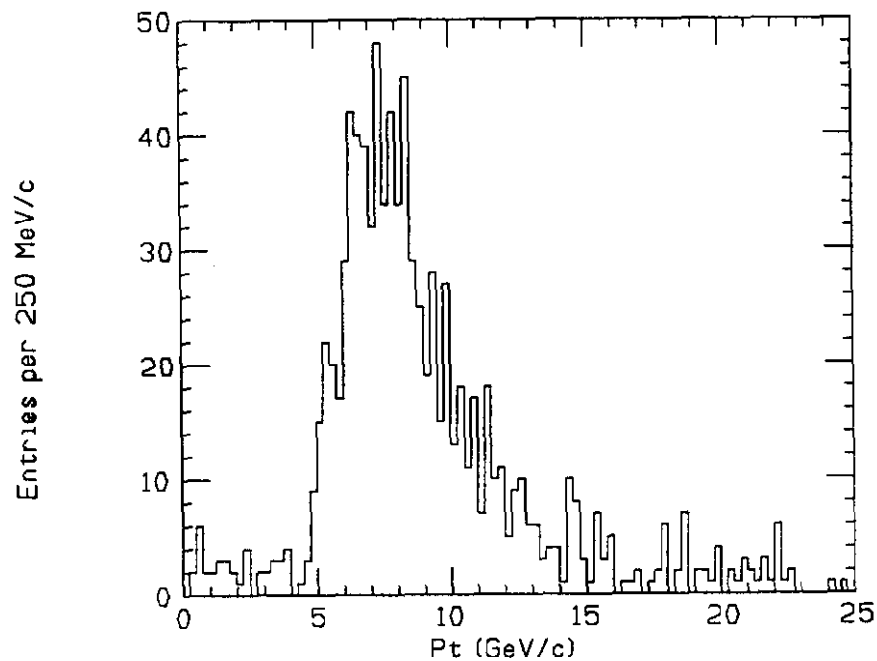


Figure 4: Reconstructed  $P_t$  of  $J/\psi$  candidates

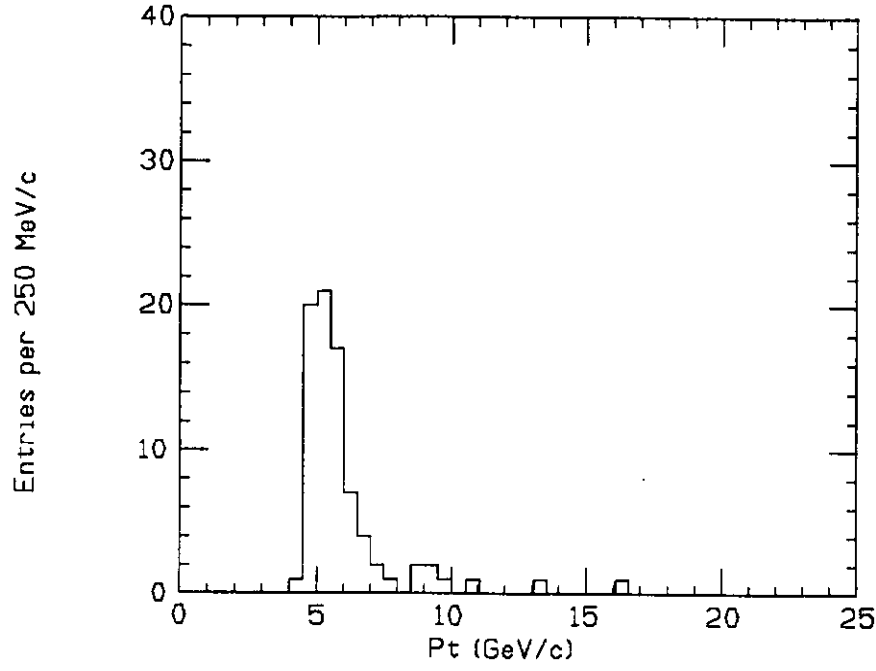


Figure 5: Highest muon  $P_t$  from  $\Upsilon$  decays

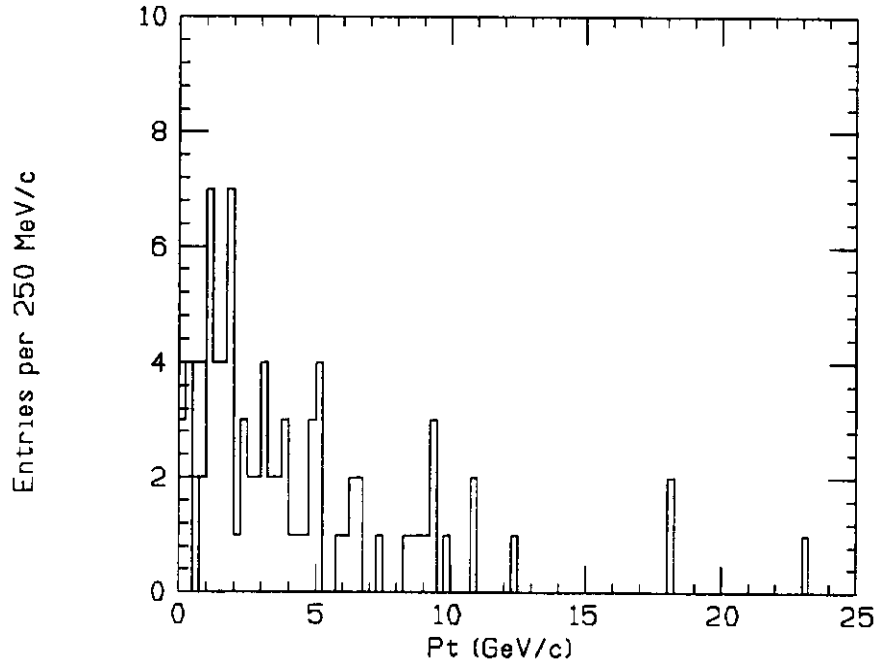


Figure 6: Reconstructed  $P_t$  of  $\Upsilon$  candidates

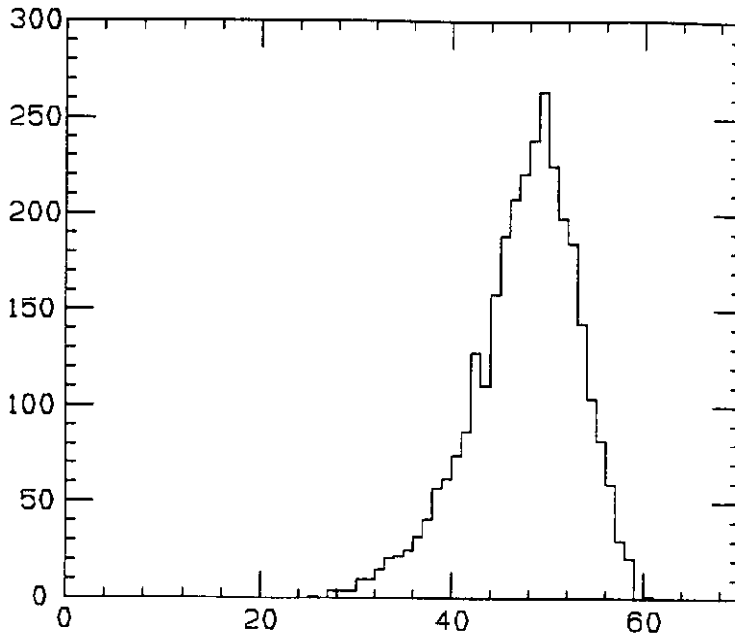


Figure 7: Number of axial hits per CTC track

## 4 $J/\psi$ and $\Upsilon$ MASSES

### 4.1 Track Quality Cuts

We studied the reconstructed masses of the  $J/\psi$  and  $\Upsilon$  in order to establish the systematic momentum scale uncertainty of the CTC. To do this we selected events only if both muons produced high quality tracks. Quality cuts are made separately on the number of axial and stereo hits on the reconstructed tracks and on the average residuals of the axial and the stereo hits. In addition a beam constraint was imposed by requiring that the tracks come from the vertex. Figure 7 shows the distribution of the number of axial hits per event and Figure 8 shows the distribution of the number of stereo hits. The cuts were placed at 45 and 16 respectively. Figures 9 and 10 show, respectively, the distribution of the mean residuals for the axial and the stereo hits. The cuts were placed at 300 microns on both axial and stereo hits.

### 4.2 CTC Calibration and Alignment

The geometry of the sense wire planes in the CTC allows a very simple self calibration procedure to be performed to determine both the drift velocity,  $V_D$ , for each superlayer, and the  $T_0$  for each track. Figure 11 shows two representative drift cells in a single superlayer of the CTC. Two hypothetical charged particle trajectories are shown as dashed lines in the figure. Focusing for a moment on the lower of the two trajectories,

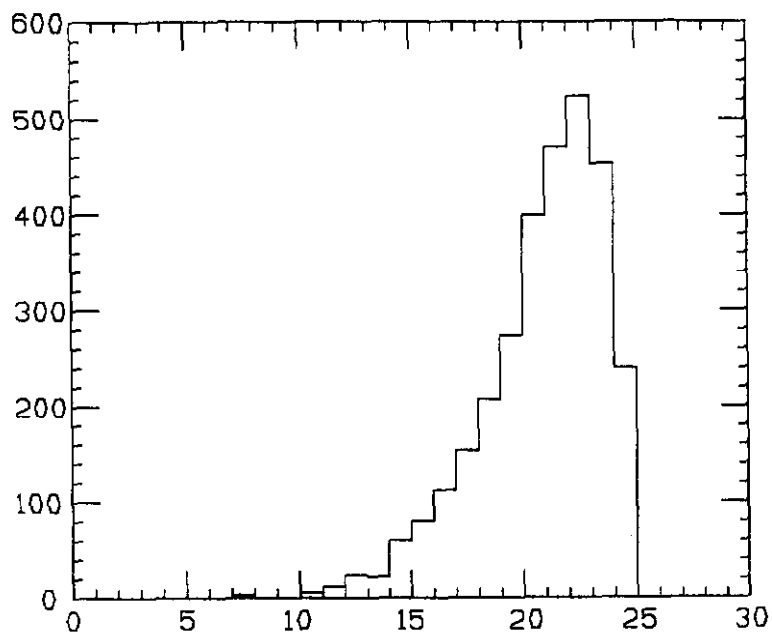


Figure 8: Number of stereo hits per CTC track

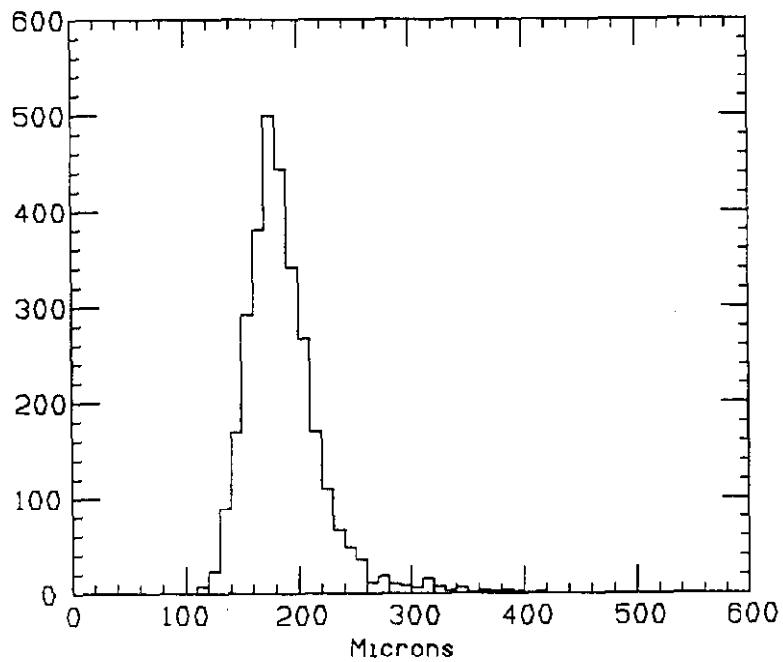


Figure 9: Average axial residuals

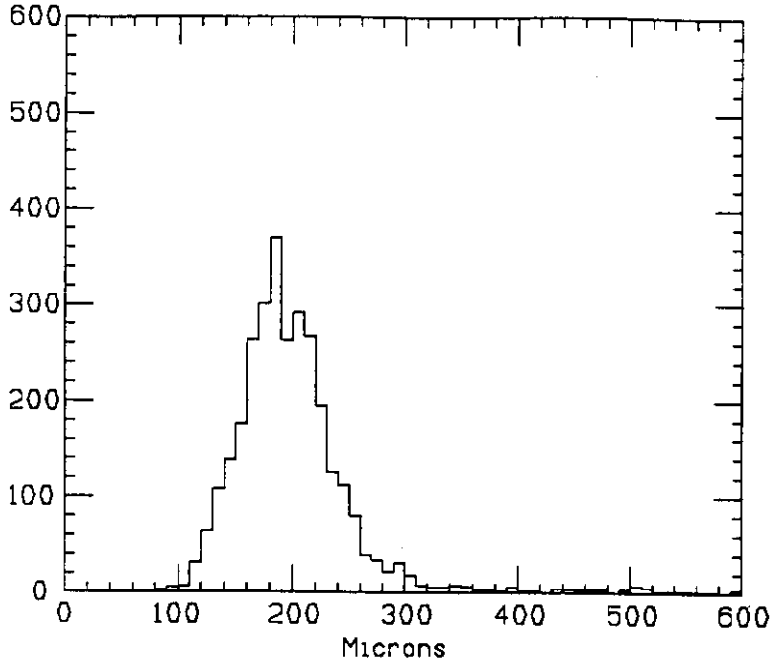


Figure 10: Average stereo residuals

we see the effect of reconstructing the track with the wrong  $T_0$ , shown as the solid lines above and below the actual trajectory, . In this case electrons drifting from both above and below will be placed too far from the sense wire plane, resulting in a discontinuity of the reconstructed track across that plane, as shown. Thus, by removing such discontinuities, we can calibrate the event  $T_0$  on a track-by-track basis.

The upper trajectory in the figure shows a particle which has traversed two drift cells in a single superlayer, as happens for 25% of all tracks. In this case the figure shows the effect of reconstructing the track using the wrong drift velocity. The result is a track which is continuous within a cell but discontinuous across cell boundaries because it has the wrong slope. By removing such discontinuities we are therefore able to calibrate the chamber drift velocity for each superlayer.

The determination of the wire positions for the tracking chamber has been performed using 800  $W \rightarrow e\nu$  events. Positrons and electrons are separated and the momentum for these tracks is fixed to the energy measured in the calorimeter. Using the resulting curvature for these tracks, the residuals for each superlayer are recalculated. Averaged over the entire sample of events the mean residuals are used to determine a rotation for each superlayer, separately for positive and negative tracks. The mean of the rotations for positive and negative tracks is used to redefine the wire positions and the procedure is iterated until the rotations are small compared to the statistical uncertainty. The rotations resulting from this procedure are of order  $10\mu$ . This procedure effectively forces positive and negative tracks to have the same average value of  $E_t/P_t$ , but does not force that value to be 1.

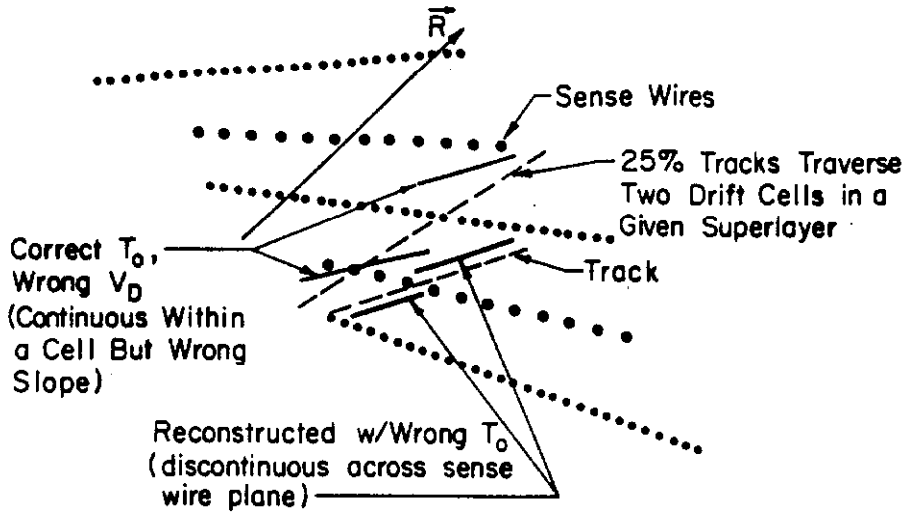


Figure 11: Self calibration of the central tracking chamber

The wire positions have been checked using cosmic ray data taken immediately following the end of the run in June 1989. Cosmic ray tracks which traverse the entire tracking chamber allow one to make two independent measurements of a single track and compare the resulting curvatures. Figure 12 shows the distribution of the sum of the two measured curvatures, normalized to the uncertainty expected from the residuals. The superimposed curve is not a fit, but a Gaussian of mean 0 and width 1. If there is a false curvature,  $Z$ , due to geometry errors, then the sum of the two measured curvatures should be equal to  $2Z$ , since the curvatures are of opposite sign. The mean of the distribution in Fig. 12 is 0.0468, equivalent to a false momentum of approximately 13 TeV/c. Such a large value for the false momentum indicates that our alignment procedure has been quite successful.

### 4.3 Mass Measurements and Implications for Momentum Precision

The masses of the  $J/\psi$  and  $\Upsilon$  are clearly known from  $e^+e^-$  experiments to a precision which will not be surpassed here. The importance of the measurement here is that it allows us to derive an upper limit on the systematic uncertainty on the mass scale in the CTC. Figures 13 and 14 show the dimuon invariant mass spectra in the region of the  $J/\psi$  and  $\Upsilon$  respectively. These data include all corrections described above, including calibrations and geometry. The measured mass values are  $3.097 \pm 0.001$  GeV/ $c^2$  for the  $J/\psi$  and  $9.469 \pm 0.010$  GeV/ $c^2$  for the  $\Upsilon$ , where the uncertainties are purely statistical. One notes a clear signal for the  $\Upsilon'$  in Fig. 14 and a slight, though not statistically significant, enhancement near the  $\Upsilon''$ .

The tracking chamber itself measures the sagitta of a track. This sagitta plus a

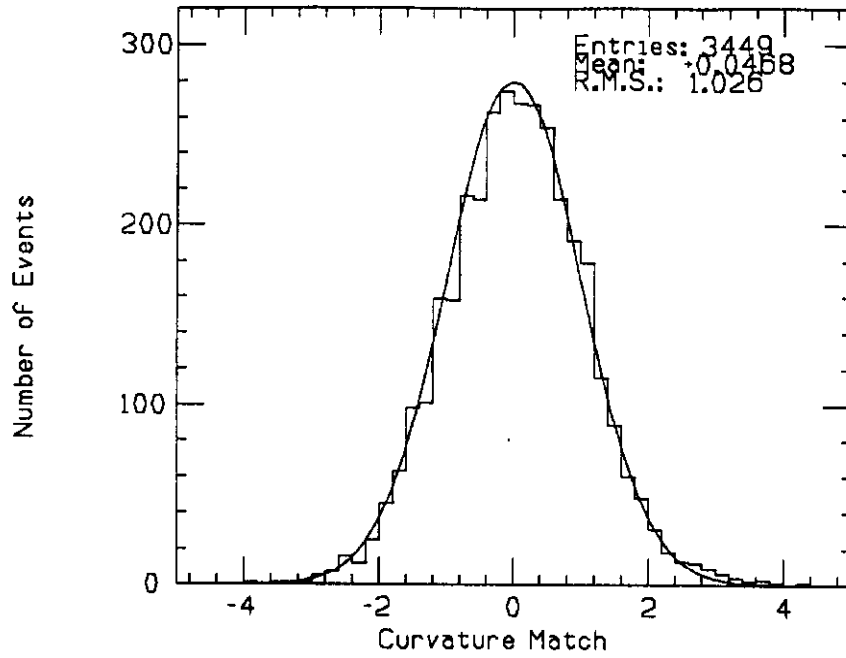


Figure 12: Mean Curvature of the Two Legs of a Cosmic Ray Track

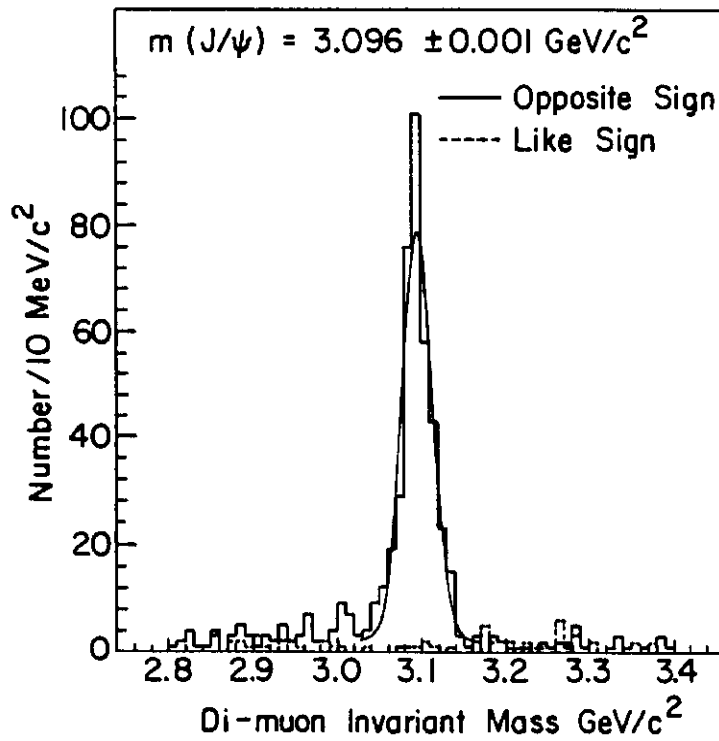
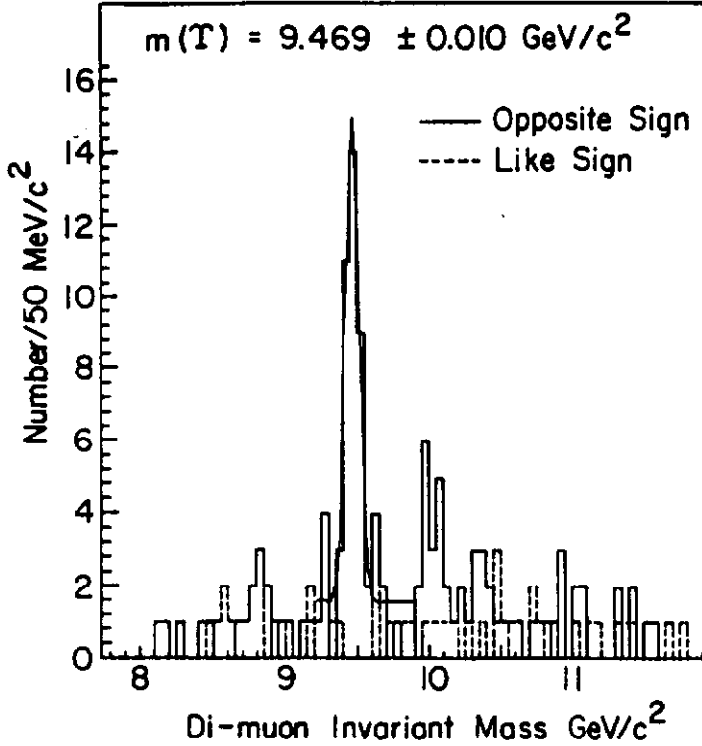


Figure 13: Fitted  $J/\psi$  peak in dimuons

Figure 14: Fitted  $\Upsilon$  peak in dimuons

knowledge of the B field and wire positions, provides a momentum. We have discussed above the determination of the wire positions. The magnetic field has been carefully mapped and measured. The axial component of the field has been found to be 1.4116T, with an uncertainty of  $\pm 0.05\%$ . The dominant contribution to the uncertainty in the field comes from the fact that the solenoid was operated at a current of 4650A, whereas it was mapped at 5000A.

It is instructive to consider the effects of errors in the measurement of the sagitta. Consider errors of the form

$$S^{meas} = k_1 \cdot S^{real} + k_2$$

where  $S^{meas}$  is the measured sagitta,  $S^{real}$  is the actual sagitta, and  $k_1$  and  $k_2$  are some constants which are 1 and 0 respectively if the measurement is perfect. If the constant  $k_1$  is not equal to 1, then it is easy to show that the mass scale will be off by the same factor. The constant  $k_2$  is somewhat more complex. Suppose  $k_2$  is a constant proportional to charge. That is,  $k_2 = qk$  where  $q = \pm 1$ . In this case the sagitta of positive tracks will shift in the opposite direction of that of negative tracks. In a two body decay, such as the  $J/\psi$  and  $\Upsilon$ , this type of error will cancel to first order. Suppose instead that  $k_2 = k$ , independent of charge. In this case the error will not cancel in two body decays. However, this is precisely the type of error which is taken out by the alignment procedure described above and which we have shown to be quite small. Furthermore, it is possible to show that a constant offset in the sagitta can be absorbed into the constant  $k_1$  above and will therefore show up in the mass scale. Given these simple arguments, it is clear that the accuracy with which we can measure the  $J/\psi$  and  $\Upsilon$  masses allows us to place an upper limit on the systematic uncertainty on the mass

scale of the tracking chamber.

Comparing our measured masses of  $3.097 \pm 0.001 \text{ GeV}/c^2$  for the  $J/\psi$  and  $9.469 \pm 0.010 \text{ GeV}/c^2$  to the world averages [2] of  $3.097 \text{ GeV}/c^2$  and  $9.460 \text{ GeV}/c^2$  we see that both measurements are within 1 standard deviation of the world average. The expected statistical uncertainty can be computed from the single track resolution

$$\frac{\Delta P_t}{P_t} = 0.0011 \cdot P_t.$$

Since the stereo reconstruction contributes very little to the statistical uncertainty, we can safely use the above equation for the statistical uncertainty in the 3-dimensional momentum. Using  $7 \text{ GeV}/c$  as a typical track momentum, then, we get

$$\frac{\Delta M}{M} = 0.707 \cdot \frac{\Delta P}{P} = 0.00078 \cdot M$$

as a statistical uncertainty on the mass for a single measurement. At the  $J/\psi$  we compute an expected statistical uncertainty of  $\frac{.235\%}{\sqrt{N_\psi}}$ , which, with over 300  $J/\psi$  events is consistent with our measured uncertainty. At the  $\Upsilon$  we expect a statistical uncertainty of  $\frac{.78\%}{\sqrt{N_\Upsilon}}$ , which, with approximately 40  $\Upsilon$  events, is also consistent with the measurement. Thus, for both measurements, the quoted statistical uncertainties are consistent with what we expect and also with the comparison to world average mass values. Taking the case with the least statistics, the  $\Upsilon$ , we see that the statistical uncertainty is approximately 0.1%. We can therefore conservatively conclude that, in these measurements, we have the sensitivity to uncover systematic mass scale uncertainties at the 0.2% level.

## 5 CONCLUSIONS

We have presented preliminary results on the characteristics of  $J/\psi$  and  $\Upsilon$  decays detected at CDF. Minimal cuts on the muons in addition to track quality cuts were made on the  $J/\psi$  sample to obtain a fitted mass of  $3.097 \pm 0.001 \text{ GeV}/c^2$ . For the  $\Upsilon$ , somewhat tighter muon cuts were required in order to bring out a significant peak. The fitted mass of the  $\Upsilon$  was found to be  $9.469 \pm 0.010 \text{ GeV}/c^2$  and a clear signal for the  $\Upsilon'$  was seen. These measurements have been used to set the systematic uncertainty on the mass scale in the tracking chamber at less than 0.2%. Work on studying the production mechanisms and production cross sections for both  $J/\psi$  and  $\Upsilon$  is currently in progress. The statistics should be considerably enhanced when the remaining  $3\text{pb}^{-1}$  of data are analyzed.

## References

- [1] F. Abe *et al.*, Nucl. Instrum. Methods Phys. Res., Sect. A **271**, 387 (1988).
- [2] See *Review of Particle Properties*, Phys. Lett. B, **204** (1988).